

A Local and Iterative Neural Reconstruction Algorithm for Cone-Beam Data

Ignazio Gallo

Università degli Studi dell'Insubria, Varese, Italy,

ignazio.gallo@uninsubria.it,

WWW home page: <http://www.dicom.uninsubria.it/~ignazio.gallo/>

Abstract. This work presents a new neural algorithm designed for the reconstruction of tomographic images from Cone Beam data. The algorithm is iterative and based on a set of neural networks that are working locally and sequentially. The algorithm was compared with the iterative ART algorithm and the filtered backprojection (FBP) method. The results show how the proposed algorithm is much more accurate even in the presence of noise and under conditions of lack of data.

1 Introduction

Cone-beam (CB) collimation has been investigated intensively since it was first introduced in the 1980. CB computed tomography (CT) can be thought of as the three-dimensional (3D) extension of the widely popular fan-beam CT. It reconstructs a 3D representation of either the entire object, or at least a thick section of it, and is thus a volumetric imaging method. Figure 1 shows a graphical representation of the CB geometry.

Cone-beam CT is very dose-efficient, as it utilizes more of the emitted X rays for image generation than fan beam, yielding a 2D projection and not just a onedimensional (1D) strip at each exposure. Moreover, due to the speedy data acquisition, motion artifacts caused by patient movement or breathing are much less of an issue than in slower forms of volumetric CT [1].

The most common algorithm used in the tomographic reconstruction of CB data is the filtered backprojection (FBP) method [2,3], invented by Bracewell and Riddle [4]. Using a large number of projections, acquired by a CT scanner, FBP produces very good results. Unfortunately, if the set of available projections is small and/or noisy, reconstructions by the FBP algorithm suffer distortions and artifacts, and only the central plane is reconstructed free of artifacts.

Several researchers [5,6,7,8] have proposed algebraic reconstruction techniques (ART) as an alternative method. In contrast to FBP, algebraic techniques are iterative, i.e. they work by iteratively updating a reconstruction grid by a projection-backprojection procedure until a convergence criterion is satisfied.

The aim of this work was to define and experimentally investigate a new iterative image reconstruction algorithm based on an adaptive neural learning technique. Salient aspects of the proposed strategy, called *Neural Star Reconstruction Technique* (NRST), is the use of a local error function. NRST works

by iteratively updating a reconstruction grid by a neural procedure until a convergence criterion is satisfied. The reconstruction task is formulated as a system of local neural networks, one for each cell of the reconstruction grid, which iteratively minimize a local error function.

The rest of the paper is organized as follows: Section 2 describes some basic concepts of image reconstruction; Section 3 introduces the proposed neural-network algorithms; Section 4 discusses the experimental results obtained by using test images with known degradation functions and comparing the method with other techniques; Section 5 outlines conclusions and future plans.

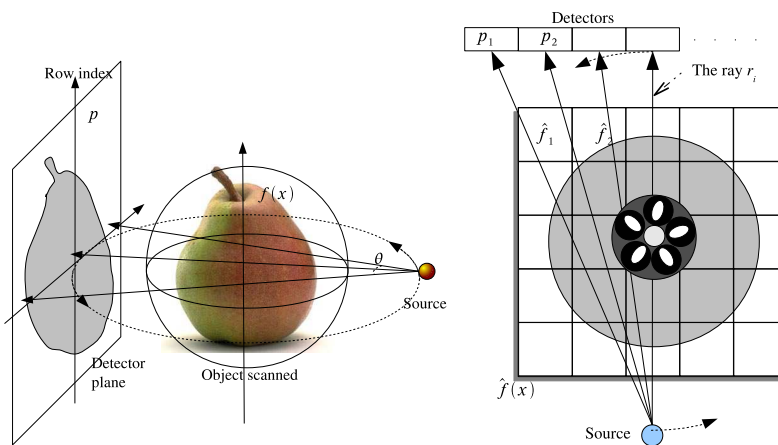


Fig. 1. Scheme of transmission tomography with a projection geometry for cone-beam data acquisition. During the scan, the x-ray source-detector assembly rotates around the object of interest and measures a set of CB projections. The goal is to compute, from this projection data, an accurate estimate $\hat{f}(x)$ of the function $f(x)$ that represents the spatial distribution of the object density.

2 Problem Statement

Tomographic imaging deals with reconstructing an image from its projections [9]. In the strict sense of the word, a projection at a given angle is the integral of the image in the direction specified by that angle. As illustrated in Fig. 1, the real image $f(x)$ has superimposed a square grid where in each cell the function is constant. Let f_j denote this constant value in the j^{th} cell, and let N be the total number of cells. For the proposed approach a ray is defined as a line running through the (x, y, z) -plane while a line integral will now be called a *ray-sum*. Let p_i be the ray-sum measured with the i^{th} ray as shown in Fig. 1. The relationship

between the f_j 's and p_i 's may be expressed as

$$\sum_{j=1}^N w_{ij} f_j = p_i \quad (1)$$

where w_{ij} is the weighting factor that represents the contribution of the j^{th} cell to the i^{th} ray-sum. Here, the factor w_{ij} is computed as the inverse of the distance d between the r_i ray and the center of the j^{th} cell (see Fig. 2).

$$w_{ij} = \frac{max - d}{max} \quad (2)$$

where normally max is equals to the pixel's size.

During the scan, the x-ray detectors rotates around the object of interest and measures a set of CB projections. The goal is to compute, from this projection data, an accurate estimate $\hat{f}(x)$ of the function $f(x)$ that represents the spatial distribution of the object density.

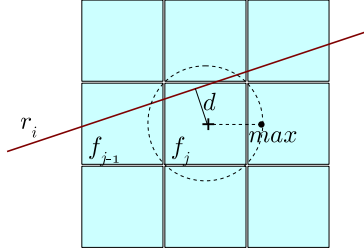


Fig. 2. The weighting factor w_{ij} represents the contribution of the cell f_j to the ray integral p_i and is computed only once as the inverse of the distance d between the ray r_i and the center of the j^{th} cell.

3 The Proposed Neural Reconstruction Algorithm

This work proposes a new iterative method, called *Neural Star Reconstruction Technique* or NRST, which uses a gradient descent algorithm to minimize a *local* cost function.

All the x-rays passing through a cell j give origin to a network R_j as that shown in Fig. 3a. R_j is a single-layer perceptron network, which consists of a single layer of output nodes; the inputs are fed directly to the outputs via a series of weights. In this way, for each x-ray generated during the scan there is a neuron having a number of inputs equal to the number of cells touched or influenced by the ray (see Fig. 3b). Each network R_j is composed by a set of neurons all passing through the cell j . While a normal perceptron like that

presented in [10] consists of a single neuron with adjustable synaptic weights and a threshold activation function, here a neuron consists of a set of fixed synaptic weights w_{ij} connecting its output to the adjustable input values \hat{f}_k .

The error measure we consider minimizing for a single network R_j is a *local* cost function E_j defined at any cell j of the volume to be reconstructed:

$$E_j = \frac{1}{2} \sum_{i=1}^{T_j} (p_i - y_i)^2 \quad (3)$$

where T_j denotes the total number of output neurons whose output value is defined as follows:

$$y_i = \sum_k w_{ik} \hat{f}_k \quad (4)$$

The weights w_{ik} are defined statically as showed in (2) while during each training iteration only the values \hat{f}_k will be updated.

The formula for the iterative update of the cells to be reconstructed is derived from (3) and (4):

$$\begin{aligned} \hat{f}_k^{new} &= \hat{f}_k^{old} - \eta \Delta \hat{f}_k \\ &= \hat{f}_k^{old} - \eta \frac{\partial E_j}{\partial \hat{f}_k} \\ &= \hat{f}_k^{old} - \eta \sum_i ((y_i - p_i) w_{ik}) \end{aligned} \quad (5)$$

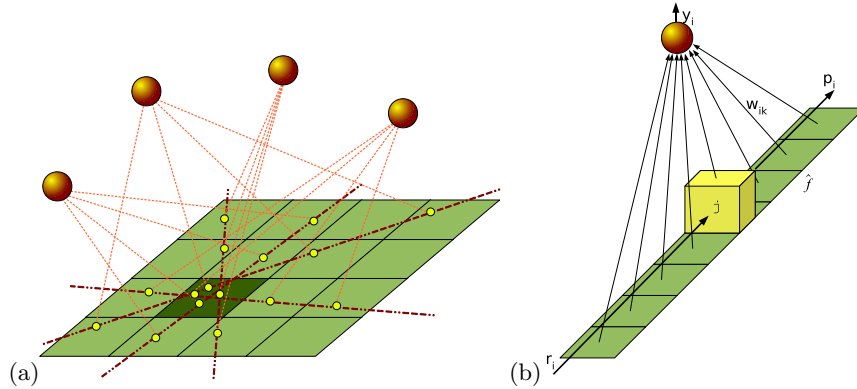


Fig. 3. A simple NSRT network R_j centered at a cell j for which a set of x-rays r_i pass (a). A single NSRT's neuron associated with the x-ray r_i having projection value p_i (b).

The method proposed in this paper consists of two main phases: the *initialization* described in the Algorithm 1, during which all the networks needed for

the reconstruction process are created and the *reconstruction* phase described in the Algorithm 2, during which the algorithm reconstructs the volume iteratively.

Algorithm 1 Initialization algorithm for creating the NSRT neural networks

Require: Acquire a set of projections $\{I_y\}$ around the real object $f(x)$ which must be scanned.

Require: Creating a NSRT neural network R_j for each cell j to be reconstructed.

Require: Each projection is formed by all truth values $\{p_i | p_i = \int_{r_i} f(x) ds\}$ given a x-ray r_i .

- 1: **for all** I_y **do**
 - 2: **for all** r_i which reaches I_y **do**
 - 3: Compute all the intersection cells G_i between r_i and the volume to be reconstructed.
 - 4: Constructs a neuron $N_i(p_i, G_i)$ associated with the x-ray r_i with truth value p_i and a set of input values G_i .
 - 5: The weight of a neuronal connection w_{ik} is computed using equation (2).
 - 6: The neuron $N_i(p_i, G_i)$ belongs to all the NSRT networks $\{R_j | j \in G_i\}$.
 - 7: **end for**
 - 8: **end for**
-

4 Experiments

The experiments presented in this section are used to study how the performance of the proposed algorithm changes when the quality and quantity of the input data change. A second set of experiments is used to compare the proposed algorithm with two other known algorithms.

The experimental work was based on a modified Shepp-Logan Phantom [11], used in Matlab, in which the contrast is improved for better visual perception (see Fig. 4a). In order to simplify the experimental work, only the phantom's slice having $z = 0$ was used. Two different types of acquisitions were used: with and without noise. In Fig. 4b-c there are two examples of sinogram without noise and with added Poisson noise respectively.

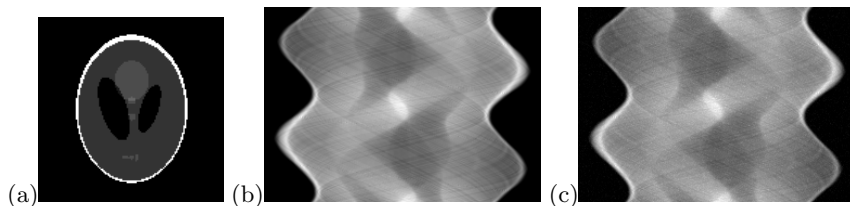


Fig. 4. Shepp-Logan Phantom used in this paper (a) and the corresponding sinogram in absence of noise (b) and in presence of Poisson noise (c).

Algorithm 2 NSRT reconstruction algorithm during a single iteration

- 1: **for all** R_j **do**
- 2: $\forall k = 1 \dots N$, $\Delta^{buf} \hat{f}_k \leftarrow 0$ and $n_k \leftarrow 0$
- 3: **for all** $N_i \in R_j$ **do**
- 4: calculating the $\Delta \hat{f}_k$ for each input cell of the neuron N_i according to (5) and add them into a buffer $\Delta^{buf} \hat{f}_k$

$$\Delta^{buf} \hat{f}_k = \Delta^{buf} \hat{f}_k + \Delta \hat{f}_k \quad (6)$$

- 5: **end for**
- 6: **for all** $N_i \in R_j$ **do**
- 7: update all the cells changed from neuron

$$\hat{f}_k^{new} = \hat{f}_k^{old} - \eta \left(\frac{\Delta^{buf} \hat{f}_k}{n_k} \right) \quad (7)$$

where n_k counts the number of increments added to the buffer $\Delta^{buf} \hat{f}_k$

- 8: **end for**
 - 9: **end for**
-

The reliability of the the reconstructed images was evaluated by Peak Signal-to-Noise Ratio (PSNR) and Normalized Mean Square Error (NMSE) given in (10) and (11) with respectively. The PSNR is most commonly used as a measure of quality of reconstruction. The signal in this case is the original data, and the noise is the error introduced by reconstruction. When comparing reconstruction algorithms it is used as an approximation to human perception of reconstruction quality, therefore in some cases one reconstruction may appear to be closer to the original than another, even though it has a lower PSNR (a higher PSNR would normally indicate that the reconstruction is of higher quality). PSNR is most easily defined via the MSE which for two $M \times N$ monochrome images f and g where one of the images is considered a noisy approximation of the other is defined as:

$$MSE = \frac{1}{NM} \sum_{i=1}^N \sum_{j=1}^M [f(i, j) - g(i, j)]^2 \quad (8)$$

$$RMSE = \sqrt{MSE} \quad (9)$$

$$PSNR = 10 \cdot \log_{10} \left(\frac{f_{max}^2}{MSE} \right) = 20 \cdot \log_{10} \left(\frac{f_{max}}{RMSE} \right) \quad (10)$$

The NMSE used for quantitative evaluation is defined by

$$NMSE = \frac{\sum_{i=1}^N \sum_{j=1}^M [f(i, j) - g(i, j)]^2}{\sum_{i=1}^N \sum_{j=1}^M [f(i, j)]^2} \quad (11)$$

In order to study the performance of the proposed algorithm different combinations of the number of projections, the number of detectors for each projection

and the size of the image to be reconstructed were used. All these configuration are showed in the Fig. 5 where the performance of the proposed algorithm is showed in terms of NMSE measure. The angle θ of the source-detector cone of x-rays was fixed to 60 degree while the relaxation parameter η and the number of iterations I were changed: in absence of noise the $\eta = 0.01$ and $I = 5$ were used while adding 36dB of Poisson noise the parameters $\eta = 0.00001$ and $I = 20$ were used.

The results showed in Fig. 5 highlight how the reconstruction quality increases with the increase in the number of detectors per projection. This remains true for the two conditions of noise considered. It is also possible to observe how with many combinations of parameters it is possible to obtain reconstructions having error NMSE close to zero. In Fig. 6 some examples of image reconstructed by the proposed algorithm.

In this experimental work a comparison analysis was performed, in which the NMSE and PSNR performances of the NSRT algorithm were compared with those obtained by the FBP and the ART reconstruction algorithms. Results obtained are summarized in Tab. 1, while in Figs. 7 and 8 there are some examples of images reconstructed by the FBP and ART algorithms. All the three algorithms were used with the same projection data and the results show that the NSRT algorithm prevails in terms of NSNR and NMSE under the different noise conditions considered but the execution time is higher. The algorithms used in this work were implemented in java obtaining an open-source library freely available for research purposes.

5 Conclusions

The CB reconstruction algorithm presented in this paper shows a better performance than the standard FBP algorithm and the basic iterative algorithms ART. The NSRT algorithm reconstructs with very high accuracy in absence of noise and remains accurate in situations with few projection data. In noisy situations the NSRT algorithm acts slightly better than the other two algorithms taken into account. For this reason the algorithm will be improved in future with new strategies for changing the input values of each network in order to optimize the results in situations of noisy projections.

One obvious disadvantage of the presented NSRT algorithm is the computational complexity, but it is important to note that the algorithm is local then this is good for future implementations in parallel.

References

1. Mueller, K., Yagel, R., Wheller, J.J.: Anti-aliased three-dimensional cone-beam reconstruction of low-contrast objects with algebraic methods. *IEEE Trans. Med. Imag* **18** (1999) 519–537
2. Smith, B.: Cone-beam tomography: recent advances and a tutorial review. *Optical Engineering* **29** (1990) 524–5341

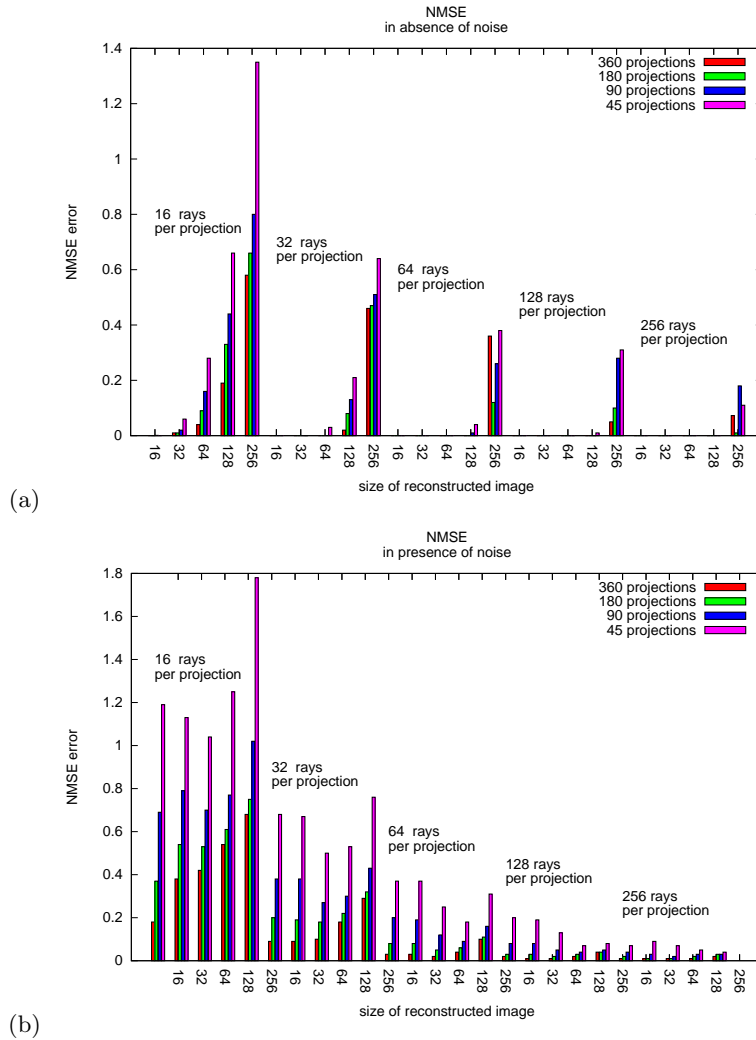


Fig. 5. NMSE error measure in absence of noise (a) and in presence of Poisson noise (b). Every plot looks at the goodness of the reconstruction varying the number of projections used by the reconstruction algorithm, the number of rays for each projection and the size of the image to be reconstructed.

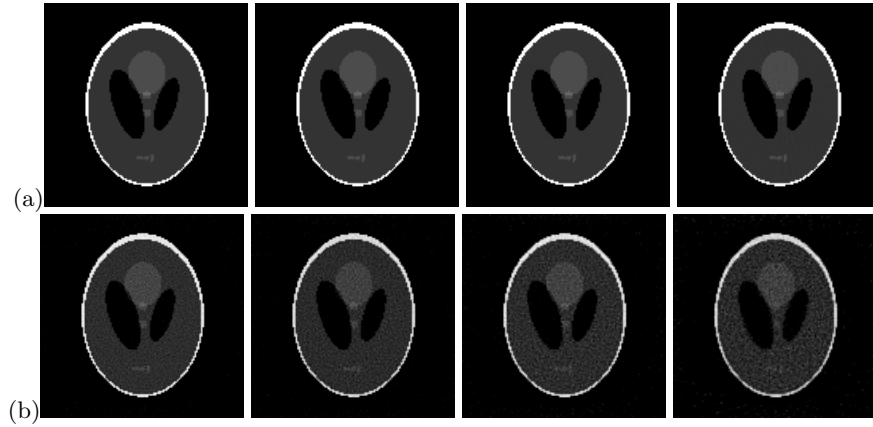


Fig. 6. Images reconstructed by NSRT algorithm in absence of noise (a) and in presence of Poisson noise (b). In each row, from left to right, the reconstructed image was obtained using 360, 180, 90 and 45 the projections respectively. The image size is 128×128 and the number of detectors used in each projection was fixed to 256.

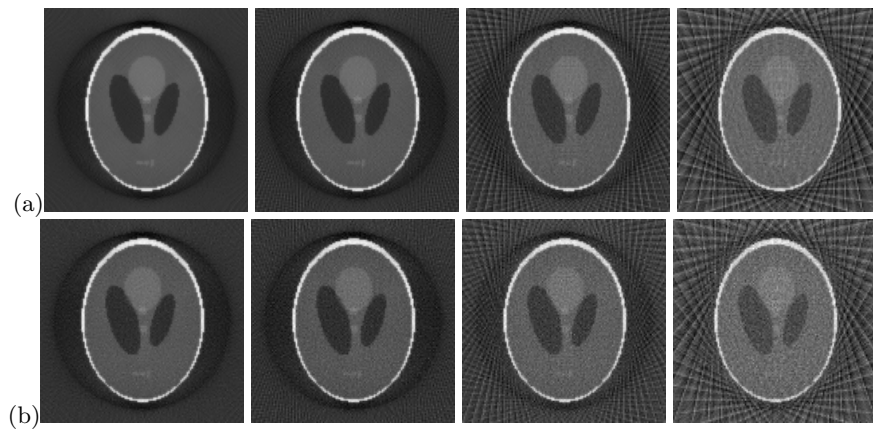


Fig. 7. Images reconstructed by FBP algorithm in absence of noise (a) and in presence of Poisson noise (b). In each row, from left to right, the reconstructed image was obtained using 360, 180, 90 and 45 the projections respectively. The image size is 128×128 and the number of detectors used in each projection was fixed to 256.

Table 1. Comparison between NSRT, ART and FBP algorithms. The numbers of x-rays and the image size was fixed to 256 and 128 respectively. Considering the FBP algorithm, the relaxation column contains the name of the filter used. The column [noise] shows the value of PSNR between the original and the noisy sinogram.

| Algorithm | Projections | iterations | NMSE | PSNR | time (sec.) | noise (dB) | relaxation |
|-----------|-------------|------------|---------|--------|-------------|------------|------------|
| NSRT | 360 | 5 | 1.8E-22 | 230.7 | 294.26 | ∞ | 0.01 |
| NSRT | 180 | 5 | 2.5E-20 | 209.31 | 125.08 | ∞ | 0.01 |
| NSRT | 90 | 5 | 2.5E-16 | 169.34 | 71.86 | ∞ | 0.01 |
| NSRT | 45 | 5 | 1.1E-04 | 52.74 | 36.85 | ∞ | 0.01 |
| ART | 360 | 5 | 0.06 | 25.28 | 12.88 | ∞ | 0.1 |
| ART | 180 | 5 | 0.09 | 23.82 | 6.57 | ∞ | 0.1 |
| ART | 90 | 5 | 0.15 | 21.6 | 3.82 | ∞ | 0.1 |
| ART | 45 | 5 | 0.28 | 19.55 | 2.45 | ∞ | 0.1 |
| FBP | 360 | 1 | 0.13 | 23.88 | 8.34 | ∞ | ramp |
| FBP | 180 | 1 | 0.15 | 23.35 | 3.86 | ∞ | ramp |
| FBP | 90 | 1 | 0.21 | 21.49 | 2.08 | ∞ | ramp |
| FBP | 45 | 1 | 0.33 | 18.73 | 1.04 | ∞ | ramp |
| NSRT | 360 | 20 | 0.01 | 33.55 | 263.23 | 36 | 1E-5 |
| NSRT | 180 | 20 | 0.02 | 31.17 | 104.58 | 36 | 1E-5 |
| NSRT | 90 | 20 | 0.03 | 28.73 | 60.94 | 36 | 1E-5 |
| NSRT | 45 | 20 | 0.05 | 26.88 | 37.16 | 36 | 1E-5 |
| ART | 360 | 5 | 0.07 | 24.91 | 12.79 | 36 | 0.1 |
| ART | 180 | 5 | 0.09 | 23.55 | 6.49 | 36 | 0.1 |
| ART | 90 | 5 | 0.16 | 21.46 | 3.58 | 36 | 0.1 |
| ART | 45 | 5 | 0.29 | 19.5 | 2.42 | 36 | 0.1 |
| FBP | 360 | 1 | 0.14 | 23.51 | 8.09 | 36 | ramp |
| FBP | 180 | 1 | 0.17 | 22.69 | 4.04 | 36 | ramp |
| FBP | 90 | 1 | 0.25 | 20.61 | 2.05 | 36 | ramp |
| FBP | 45 | 1 | 0.38 | 17.85 | 1.09 | 36 | ramp |

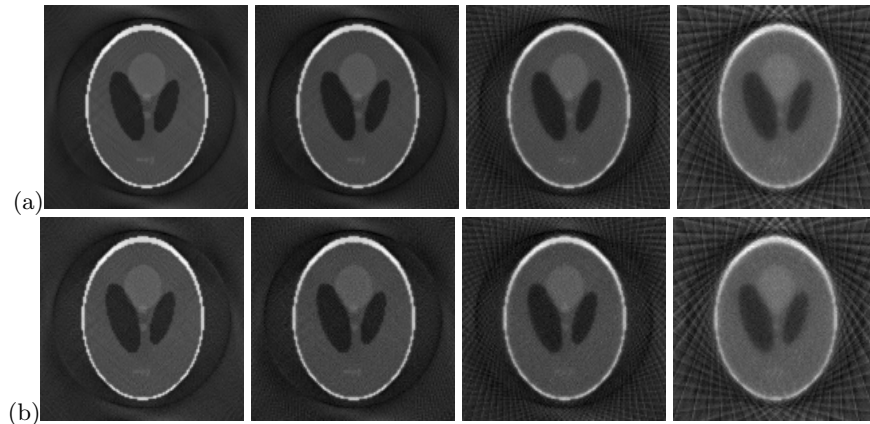


Fig. 8. Images reconstructed by ART algorithm in absence of noise (a) and in presence of Poisson noise (b). In each row, from left to right, the reconstructed image was obtained using 360, 180, 90 and 45 the projections respectively. The image size is 128×128 and the number of detectors used in each projection was fixed to 256.

3. Wang, G., Lin, T., Cheng, P., Shinozaki, D.: A general cone-beam reconstruction algorithm. *IEEE. Trans. Med. Imag.* **12** (1993) 486–496
4. Bracewell, R.N., Riddle, A.C.: Inversion of Fan-Beam Scans in Radio Astronomy. *Astrophysical Journal* **150** (November 1967) 427–434
5. Herman, G., Meyer, L.: Algebraic reconstruction can be made computationally efficient. *IEEE. Trans. Med. Imag.* **12** (1993) 600–609
6. Mueller, K., Yagel, R., Wheller, J.J.: Fast implementations of algebraic methods for three-dimensional reconstruction from cone-beam data. *IEEE Trans. Med. Imag.* **18** (1999) 538–548
7. Jiang, M., Wang, G.: Convergence of the simultaneous algebraic reconstruction technique (sart). *IEEE Transactions on Image Processing* **12** (2003) 957 – 961
8. Dennerlein, F., Noo, F., Hoppe, S., Hornegger, J., Lauritsch, G.: Evaluation of Three Analytical Methods for Reconstruction from Cone-Beam Data on a Short Circular Scan. In *IEEE*, ed.: 2007 IEEE Nuclear Science Symposium Conference Record. (2007) 3933–3938
9. Kak, A.C., Slaney, M.: *Principles of computerized tomographic imaging*. Society for Industrial and Applied Mathematics (2001)
10. Rosenblatt, F.: The perceptron: a probabilistic model for information storage and organization in the brain. *Psychological Review* **65**(6) (November 1958) 386–408
11. Shepp, L.A., Logan, B.F.: The fourier reconstruction of a head section. *IEEE Trans. Nucl. Sci.* **NS-21** (1974) 21–43